Fracture and *R*-curves in high volume fraction Al_2O_3/Al composites

N. Nagendra and V. Jayaram

Department of Metallurgy, Indian Institute of Science

Bangalore 560 012, INDIA

ABSTRACT

Fracture toughness and fracture mechanisms in Al_2O_3/Al composites have been described. The unique flexibility offered by pressureless infiltration of molten Al-alloys into porous alumina preforms has been utilised to investigate the effect of microstructural scale and matrix properties on the fracture toughness and the shape of the crack resistance curves (*R* - curves). The results indicate that the observed increment in toughness is due to crack bridging by intact matrix ligaments behind the crack tip. The deformation behaviour of the matrix, *which* is shown to be dependent on the microstructural constraints is the key parameter *that influences* both the steady state toughness and the shape of the *R*-curves. Previously proposed models based on crack bridging by intact ductile particles in a ceramic matrix have been modified by the inclusion of an experimentally determined plastic constraint factor (P) that determines the deformation of the ductile phase and are shown to be adequate in predicting the toughness increment in the composites. Micromechanical models to predict the crack tip profile and the bridge lengths (L) correlate well with the observed behaviour and indicate that the composites can be classified as i) short range toughened and ii) long range toughened based on their microstructural characteristics.

1. INTRODUCTION

Ductile phase reinforced ceramics [1-5], interpenetrating phase composites [6-8] and metal matrices with high volume fraction of ceramic reinforcements (> 50%) [9, 10] are emerging as important classes of materials with potential for structural applications requiring high specific modulus, strength and toughness. The high strength and toughness in these materials are shown to be a direct consequence of energy dissipating toughening mechanisms that reduce the crack driving force at the crack tip [11]. Although fracture behaviour has been studied extensively; *the contribution of any single mechanism to increasing the crack resistance is rather difficult to estimate,* and a dominant mechanism is often known to mask the effect of other operating mechanisms. The predominant mechanism of strengthening and toughness enhancement in these classes of composites has been identified as bridging of flaws and cracks by intact ductile phase in the wake zone behind the crack tip [12, 13]. The bridging ligaments exert closure stresses which reduce the stress intensity at the crack tip and offer resistance to further crack opening or propagation (R - curves). Thus, in such materials that exhibit wake controlled toughness behaviour, it is observed that the applied load and the crack opening displacement (COD) are strongly coupled and the COD measurement for predicting crack length becomes functionally dependent on specimen geometry and distance from the crack tip. As shown in figure 1 a single crack is observed to start from the notch *with* bridges in the wake of the crack tip. Initially, the length of such a wake zone (L_o) is identical with the distance between the crack tip and notch tip. An increase in the length of this shielding wake zone necessarily diminishes the driving force at the crack tip, i.e., an increase in macroscopic crack resistance is measured with crack extension. With further crack propagation, the wake zone length follows the crack tip until a plateau-like saturation (steady-state toughness) in resistance is reached, corresponding to a critical amount of COD. In earlier work, the R-curve was assumed to be a material property. Later, it was observed that there is no unique R-curve for these materials, i.e., the shape of the

curves and the increase in crack resistance depended on the depth and location of the initial crack, specimen dimension, testing conditions and evaluation method [14-20]. In ceramic-metal composites, the shape of the R- curve was also found to be dependent on the deformation characteristics of the bridging ductile ligaments. The toughening contribution by plastic deformation of the ductile phase is governed by the yield strength of the ductile constituent, the debonding at the matrix/particle interface and the uniaxial flow stress under constraint imposed by the rigid brittle phase. The changes in unaxial stress, σ, of the bridging ligament with crack opening, *2u,* can generally be represented by a stress displacement function $\sigma(u)$, which uniquely describes the ligament *deformation* characteristic [21]. The shape of the $\sigma(u)$ function determines the way in which the crack resistance develops as the crack grows and thus controls the final steady state toughness. A general schematic representation of the different $\sigma(u)$ function of ligaments with high and low levels of mechanical constraint is shown in figure 2 [22]. If the mechanical constraints for the deforming ligaments are high, the corresponding peak stresses are high (approximately 18 times of the initial matrix strength σ_o) as observed in the case of fine particles [23] and final fracture occurs at relatively lower critical extension, *2u**. Conversely, if the mechanical constraints are lowered either due to larger debonding, premature fracture of the brittle phase or coarse *microstructural scale in* the matrix, the peak stresses in the ligament tend to be closer to the initial matrix strength σ_o but fracture occurs at higher 2u*. The overall energy observed is thus a combination of both the peak stress σ_y and 2u* and can be approximated by the area under the $\sigma(u)$ curve.

Previously reported work on toughening by ductile constituents embedded in a brittle phase has been on materials processed through routes such as directed melt oxidation [24, 25], pressure infiltration [26, 27], reactive melt penetration [28], etc. and are restricted to a narrow range of microstructure scale, either in particle size or in volume fraction. Pressureless infiltration of molten alloys into porous ceramic preforms, on the other hand, enables the

fabrication of composites to near-net shapes with unique flexibility in fabricating composites with highly controlled and diverse microstructures with respect to the size, aspect ratio and volume fraction of both ductile and brittle phases [29-32]. In addition, by varying the process conditions it is possible to tailor the matrix to be either predominantly alloy [29] or an interpenetrating structure with another brittle constituent (AlN) [33]. The present work is an investigation on the fracture toughness of Al_2O_3/Al -AlN composites fabricated by pressureless infiltration of Al-alloys into preforms of alumina. *An attempt has been made to determine and explain the shape and spatial extent of the R-curves displayed by these composites with wide variations in microstructural scale and in matrix flow stress*. Existing quantitative and qualitative models based on crack bridging by intact ductile ligaments have been extended to *predict* the observed trends in crack resistance of the composites. This paper deal specifically with the role of physical microstructural variables, i.e. particle size and volume fraction. A companion paper examines the effect of phase changes induced by ageing treatment and the presence of AlN in the matrix.

2. EXPERIMENTAL PROCEDURE

Material

Al_2O_3/Al composites were fabricated to near-net shape by pressureless infiltration of Al-Mg-Si alloy (Al-5.5Mg-6.6Si-0.35Fe) into alumina preforms at 900°C in N_2 atmosphere [34]. The net-shaped preforms were made by cold pressing and sintering of alumina powder. The microstructures of the resulting composites are shown in figure 3 (a-d). To reduce the volume fraction to ~30 % of particulate in the composite, *preforms were* prepared using base alloy powder as the binder. The actual volume fraction and mean size of the particulates in the composites *were* measured by an image analyser attached to an OLYMPUS microscope and are

given in table 1. Compact tension (C-T) specimens of dimensions 16 x 15 x 6.5 mm. were cut from the fabricated composites in a direction transverse to the infiltration direction and ground to *their final dimensions*. The specimens were homogenised at 500°C for three hours prior to quenching in air and one of the surfaces *was* polished to a finish of 1μm to facilitate observations of pre-cracking and crack growth.

Fracture testing

The specimens were notched *straight through* with a diamond blade of 0.3 mm thickness in a high speed diamond saw and a stable pre-crack was introduced by *the bridge indentation* technique [35]. Fracture toughness measurements were performed according to *ASTM E399* specifications. However, for crack growth studies, the initial crack length was restricted to 0.2W and crack growth was monitored from changes in specimen compliance by a clip gauge (resolution of 0.1μm) that measured the crack opening displacement (COD). The COD measured between two knife edged stubs attached to the crack surface (Fig. 4) was calibrated *through the use of specimens* with known crack lengths in the composite. A typical compliance curve for predicting crack length is shown in figure 5 along with the *computed variation for this geometry [*36]. Tests were carried out in a screw-driven Instron under displacement control at a crosshead speed of 6μm/min. and the specimen was loaded to failure. The fractured surfaces were examined by scanning electron microscopy (SEM - JEOL 840 SM). *In some cases the* test was interrupted and the sample was examined in the SEM to observe the microstructural changes during crack growth.

3. RESULTS

The fracture toughness values of the Al_2O_3/ Al composites processed by pressureless infiltration of Al-alloy into alumina preforms in the temperature range of 900-1000°C were measured to be in the range of 9-16 MPa√m (table 1). The toughness of the composites decreased with increasing particulate volume fraction, except in sample C_1 which had higher bulk porosity due to settling and segregation of particles during processing [33]. However, at a given volume fraction, the particle size was not found to have a significant effect on the toughness of the composite. A typical load vs. COD trace of the specimen during crack growth studies is shown in figure 6. The *R*-curves for the composites computed from the load vs. COD data were observed to start from ~ 2-4 MPa√m which *is close to* the intrinsic toughness of the microstructure, and reached a final toughness values of 9-19 MPa√m after stable crack growth (Fig. 7 a-b). The shape of the crack resistance curve, however, showed a marked dependence on the microstructural scale. In composites with a fine microstructure or a higher volume fraction of particulate, the crack resistance rose sharply and began to flatten at short crack extensions; while in composites with a coarser microstructure or smaller particulate fraction the onset of steady state behaviour was reached at larger crack extensions. The crack growth characteristics of all the composites were observed to be similar, irrespective of the microstructural parameters. The crack growth behaviour indicated various operating toughening mechanisms. However, features such as crack deflection/meandering or micro-cracking of the reinforcing particle ahead of the crack tip were on a small scale and their contribution to the overall toughness was masked by the predominant toughening mechanism of crack bridging by intact matrix ligaments. SEM observations of crack growth and the crack tip revealed the formation of matrix *ligaments bridging* the two crack surfaces as shown in figure 8. The crack was observed to have circumvented the matrix by advancing continuously into the particle/matrix interface or into the brittle reinforcement particles. The intact matrix was observed to be present as bridges holding

the crack surfaces over appreciable distances (of up to 5 mm. in composite E), thus, forming a bridging zone. Once the bridges were formed, the deformation behaviour of the intact metal ligaments behind the crack tip (Fig. 9) was observed to be crucial in controlling further toughening in the composite. The deformation and flow behaviour of the metal ligament embedded between elastic particles is observed to be strongly dependent on the nature of the interface between matrix/particle and the physical constraint imposed by the intact elastic particles of alumina. Since strong bonding is expected between Al_2O_3/Al-Mg alloys, the constraints are dependent on the microstructural parameters of the composite.

Fracture mechanisms

Particle failure

The crack front was observed to be attracted towards the particles, leading to the nucleation of secondary cracks or voids at the particle/matrix interface. Since, the interfacial bond strength is expected to be high, the crack entered the particles leading to particle fracture (Fig 10 a). The extent of micro-cracking and particle fracture scaled with the size and inversely with the strength of the reinforcing particle. Incidence of cleavage in the reinforcement particles (Fig. 10 b) became more evident in composites with particle size above a critical size of ~23μm and at equivalent particle size in the fused and porous alumina.

Matrix failure

A study *was made* of the relative constraints imposed on the matrix by the largely elastic particles by indenting the matrix and measuring the induced displacement in a dynamic ultra low load micro hardness tester [34]. The indent size was chosen to be approximately 60 % of the matrix spacing and the plastic zone thus formed was calculated [37, 38] from the load-displacement curves.

$$\left(\frac{c}{h}\right)^3 = 3.639\left[\frac{(E/Y)\tan\beta + 4(1-2\upsilon)}{(1-\nu)}\right] \qquad \textbf{(1)}$$

where "*c*" is the plastic zone radius, h the depth of plastic penetration, *E, Y* and ν the elastic modulus, yield strength and Poisson's ratio of the indented material, and β is the cone angle of an equivalent conical indentor. Assuming the properties of the base alloy as *E*= 69 GPa, *Y* = 276 MPa (6061 - Al-Mg-Si alloys), ν = 0.33 and β = 19.69° for the indentor in use, the measured plastic penetration gave an *estimate of the* plastic zone radius from equation (1). The ratio of the plastic zone formed in the base alloy to that in the composite matrix was thus assumed to be a measure of the *constraint exerted on the deformation of the matrix by the elastic* particles. The relative plastic constraints experienced by the matrix during deformation are given in table 1.The changes in the matrix deformation behaviour *during fracture* with changes in the relative plastic constraint are shown in figure 11 (a-f). In composites with very fine particulates or high particulate volume fraction (low interparticle spacing and/or high constraint), the observed matrix deformation *is typified by* figure 11 (a, b and e). *The deformation in composites with moderate constraint and interparticle spacing is shown in* figure 11. (c, d and e). In composites with large interparticle spacing and low constraint, deformation was by extensive void nucleation and coalescence typical of *the fracture surface* shown in figure 11 (h).

4. ANALYTICAL MODELLING

The common feature of the toughening observed in the composites studied is the presence of matrix *ligaments that bridge* the crack surfaces. The various aspects of crack bridging parameters and the measurement of crack opening displacement at steady state toughness are illustrated in figure 12.

4.1 Matrix contribution to composite toughness

Assuming that linear elastic fracture mechanics (*LEFM)* still holds, the stresses surrounding the bridged crack can be expressed by stress intensity factor notation. Thus, the equilibrium crack configuration with an applied stress intensity factor K_A , crack length c and a crack length dependent fracture toughness $K_R\ (c)$ can be written as [28]

$$K_A = K_o + \sum_i K_{\mu i}(c) = K_R(c) \qquad \textbf{(2)}$$

where, K_o is the crack tip toughness and $K_{\mu i}$ is the toughness from the microstructure which *arises out of the sum of all the crack closure stresses p(u) that come about* by bridging of the crack. The crack closure stresses are a function of the crack opening displacement (COD), *2u,* and hence change with crack length. Rewriting in terms of the mechanical strain energy release rate, *G,* that implicitly includes closure stresses as a function of COD, the equation assumes a form as

$$G_A = R_o + \sum_i R_{\mu i}(c) = R(c) \qquad \textbf{(3)}$$

where, $G_A = R(c)$, the composite crack resistance, R_o is the crack tip resistance and $R_{\mu i}$ is the crack resistance from the microstructure *that is* dependent on *p(u)*. The stress-displacement function uniquely describes the matrix characteristics and is *known* to be responsible for the increasing fracture resistance with increasing crack length. *Thus, the toughening contribution due to plastic deformation of the matrix alloy is* governed by the mechanical properties of the alloy, the interface properties, matrix ligament diameter and volume fraction. In cases where intercrystalline fracture of the reinforcing particles is observed , interlocking grains remain in contact across the crack faces and possibly form frictional bridges *that provide* additional crack

closure stresses.

In the elastic or elastic-plastic case under small scale yielding condition, the stress intensity factor can be related to the strain energy release rate by

$$G_A = \frac{K_A^2}{E\left(1-\nu^2\right)} \qquad \textbf{(4)}$$

where E is the composite elastic modulus.

Combining Eqs. (2) through (4), the fracture toughness at the plateau of the *R*-curve K_{ss} , *obtained* at a crack length c_{ss} where the first active bridge fails can be written as

$$K_{ss} = \left[K_o^2 + ER_{\mu,\text{particles}} + ER_{\mu,\text{metal}}(c)\right]^{1/2} \qquad \textbf{(5)}$$

where $K_o = \sqrt{(R_o E)}$ is the crack tip toughness of the composites. *Observations of the fracture surface* reveal that in all the composites, the alumina particles fracture essentially in a transgranular manner. Accordingly, the toughening contribution by elastic bridging can be neglected and equation (5) can be reduced to

$$K_{SS} = \left[K_o^2 + ER_{\mu,\text{metal}}(c)\right]^{1/2} \qquad \textbf{(6)}$$

4.2 Prediction of steady state toughness

When fracture resistance is dominated by plastically deforming bridging matrix ligaments, the stress/stretch function associated with these ligaments, σ_b *(u),* is the key composite property. Assuming that σ_b *(u) is softening dominated* [39], the relation can be approximately reduced to [40]

$$\sigma_b \approx \sigma_y \ (1-u/u^*) \qquad \textbf{(7)}$$

where u is the crack opening displacement and σ_y and u^* are constants to be determined

either by experiment or by calculation. Furthermore, it is imperative that σ_y be a multiple of the uniaxial yield strength of the base alloy σ_o.

The toughening increment due to crack bridging by a ductile reinforcement can be estimated from

$$\Delta G_{SS} = A_f \sigma_y R_{eff} \chi \qquad \textbf{(8)}$$

where ΔG_{SS} is the steady-state toughness, A_f is the area fraction of the matrix on the crack plane ($1-V_f$), σ_y is the uniaxial yield strength of the matrix ligament (= P σ_o), R_{eff} is the effective radius of cross section of the matrix, while χ is a "work -of-rupture" parameter for the matrix. The parameter χ is defined as [41]:

$$\chi = \int_0^{u^*/R} \frac{\sigma(u)}{\sigma_y} d\frac{u}{R} \qquad \textbf{(9),}$$

where $\sigma(u)$ is the nominal stress, u the crack opening displacement and u^* the crack opening displacement upon ductile phase failure. χ can be empirically related to the plastic stretch of the matrix ligament u^* [41, 42] as $2u^*/R$. From fracture analysis of the crack surfaces in the composite material, u^*/R can be obtained by measurement of the deformed ligament in profile (Fig. 12) [40]. Experimental evidence by previous workers [42] have indicated that there is no systematic dependence of u^*/R on R and χ can be evaluated from the relationship between χ and u^*/R obtained by Ashby *et. al.* [41]. The steady-state toughness can thus be calculated as

$$K_{SS} = \left\{ K_o^2 + E\left(1 - \nu^2\right) \Delta G_{SS} \right\}^{1/2} \qquad \textbf{(10)}$$

The model discussed above can be applied in a straightforward manner to predict the toughness of the composites by knowing the yield strength of the base alloy and the yield strength of the

matrix ligament. However, in the present study, the base alloy that has been used for processing is of a non standard composition and by assuming the uniaxial yield strength (σ_o) of 276 MPa (6061 alloys) for the base alloy, the uniaxial yield strength of the matrix (σ_y) can be calculated as $\sigma_y = P\sigma_o$, where P is a factor relating the constraint imposed by the microstructural parameters to the strength of the alloy. The plastic stretch to failure of the bridging matrix ligament u^* can be estimated from a high angle tilt SEM image of the fractured matrix ligament and by assuming that the initial matrix radius is *half the inter-particle spacing* (d'_i). Thus, the steady state toughness (K_{SS}) *may be* calculated from equation 10. For example, composite C_3 (avg. particle size 23μm, V_f~0.61) had a matrix content of 0.39 with an initial matrix radius of 4.5 μm and yield strength σ_y = 387 MPa. From post-fracture analysis the effective plastic stretch in matrix ligaments prior to failure (u^*) was measured as 3μm giving a normalised plastic stretch (u^*/ R_{eff}) of 0.67. The computed value of χ from [41] was 1.63. Substituting the values in equation 10 and the composite modulus as 195 GPa, ν = 0.28 [43] and K_o = 4 MPa√m, the steady state toughness values is calculated as 14.5 MPa√m while the measured steady state toughness from K_R - curves showed 16 MPa√m (table 2). A comparison of experimentally observed and predicted fracture toughness is made later.

4.3 Modelling of crack-tip profile

A micromechanical model from quantitative measurements of the crack displacements and the near-tip crack profile can be used for a comparative study of the observed variation in independently measured fracture toughness (K_Q) and steady state toughness (K_{SS}) from crack growth studies. For this the crack opening displacements (COD, $2u$) for the compact-tension specimen geometry are theoretically computed from measurements at a distance x behind the crack tip as indicated in the schematic diagram (Fig 12) and the Irwin K-field plane strain displacement relation [44] that is assumed to represent the near-tip profiles for *stress-free* crack

surfaces as

$$u(x) = (8x/\pi)^{1/2} K_A / E' \qquad (11)$$

where $E' = E / (1-\nu^2)$ in plane strain, E *is* the Young's modulus of the composite material, ν is Poisson's ratio (= 0.28 [43]) and K_A (or K_Q) is the applied stress intensity factor. Equation (11) is expected to remain a reasonable approximation for non bridged cracks extending from sufficiently long notches ($\Delta c \ll c_o$ as shown in Fig. 12) and a parabolic data fit can thus be used to determine K_A [21] of a material. In material that shows no R-curve behaviour (ex. brittle materials such as glass etc.) the K_A thus determined is found to be nearly equal to the material property K_{Ic}. But in materials that show a rising R-curve due to bridging, a strong modifying influence on the crack profile is exerted by the bridging tractions and the profile is not determined by a single value of K_A . In such materials, the steady state toughness of the rising R-curve can be argued to lie within the bounds defined by a set of asymptotic parabolas computed from equation 11. The lower bound is computed from the assumed crack-tip toughness ($K_A = K_o$), while the upper bound computed from the toughness at the notch-tip ($K_A = K_Q$) evaluated from the externally measured loads and the known stress intensity solution for the specimen geometry.

In the present case, the crack-tip profile computed from an assumed crack tip toughness ($K_A = K_o$) of 4 MPa√m, is observed to be nearly independent of the microstructural scale of the composites and is designated as the lower bound. Calculation of the crack-tip profile for two extreme scales of microstructure : $K_A = K_Q =$ 9 MPa√m in composite E (180μm and $V_f \sim$ 0.64); and $K_A = K_Q =$ 11.4 MPa√m in composite A (<1μm and $V_f \sim 0.56$) can thus be designated as the upper bounds for toughness observed in this class of composites. The computed crack profiles are parabolic and are shown in figure 13. The crack profile in a composite with coarse microstructure shows a large extent of crack growth to reach a critical COD, while in the fine-scale composite, an increase in critical COD is observed at nearly half

the crack growth observed in the coarse composite. The profile can be argued to be reflective of the observed rise in fracture resistance with crack growth (K_R - curves) with variation in the scale of microstructure.

4.4 Calculation of bridge-zone length(L)

The contribution of matrix ligament fracture to the overall resistance to crack extension may be estimated by assuming that the crack has to propagate through the compressive bridge zone of length *L*. The critical crack opening displacement *2u** should thus correspond to the elongation of the furthest (from the crack tip) matrix ligament in the bridging zone. At the moment of fracture of the matrix ligament, the critical extension *2u** can be related to the bridging zone length *L* by the expression [45]

$$L = \frac{\pi}{8} \frac{E^2 u^{*2}}{\left(1 - \nu^2\right)^2 K^2_0} \qquad \textbf{(12)}$$

where *E* is the Young's modulus of the matrix ligament assumed to be equal to *that of* the base alloy, ν is the Poisson's ratio of the matrix (0.33), *u** is the measured elongation to failure of the matrix and K_o is 4 MPa√m (crack tip toughness). The computed bridge zones from the equation 12 are tabulated in table 2. As expected the bridging zone formed behind the crack tip is strongly dependent on the microstructural scale and the matrix heat treatment.

5. DISCUSSION

The rise in fracture resistance upon crack extension can be attributed to the crack growth characteristics by assuming that the initial crack tip toughness, K_o , is independent of initial crack length c_o, and that the crack starts to extend when the remotely applied K_A, reaches the value of K_o. In particulate composites, three types of basic fracture [46] are possible. With the onset of crack growth, the associated high stresses at the crack tip lead to yielding with limited plastic straining in the matrix until the crack reaches the particle/matrix interface. Upon expanding the plastic strain in the matrix, plastic flow involves opening of the crack at the interface and propagation of the crack occurs at a lower stress intensity level along the particle/matrix interface (type 1). If the interface *and the matrix are strong, the crack enters the particles resulting in their being loaded to their fracture stress followed by cracking* (type 2). If the matrix strength is weak relative to the interfacial and particle strength, fracture occurs in the matrix by normal void nucleation and growth (type 3). A different crack growth mechanism involves particle micro cracking at sites ahead of the crack tip where the tensile stresses are the highest. The micro-cracks coalesce to become a macroscopic crack perpendicular to the applied stress and leaves intact matrix ligaments behind the crack tip as has been observed in matrices with higher reinforcement volume fraction of particulates (>20%) [47].

The observed crack resistance curves of the composites showed significant differences when compared to figure 1 and the independently measured fracture toughness of the composites are observed to lie either below or near the plateau of the *R*-curve (represented as K_{ss}). In the present study, the crack tip toughness, however, could not be estimated as their measurements require precise measurements of COD very close to the crack tip. *In-situ* observation of crack growth in a SEM by various workers have shown K_o to be ~2 $MPa\sqrt{m}$ for alumina [21] and ~2-4 $MPa\sqrt{m}$ in Al_2O_3/Al composites [24, 25, 40]. Thus it is probably reasonable to assume that K_o is ~ 3-4 $MPa\sqrt{m}$ for the composites studied. Assuming that the

crack tip toughness (K_o) is the same for all the composites studied, further toughening can be attributed to the plastic deformation and failure sequence in the crack bridging ductile matrix ligaments.

The deformation and failure sequence in the matrix are significantly influenced by the their morphology and volume fraction. The composites were processed by a base alloy rich with Mg (6%) which forms a strong interfacial bond with the alumina particles at the processing temperatures employed. The matrix deforming under constraint from the strongly bonded particles shows a near absence of dimpled rupture as expected in ductile fracture, but deforms as ridges which are nearly continuous between the particles. The formation of ridges indicates that considerable plasticity is occurring in the matrix but is very limited in the volume of material involved. Thus, under very low loads, the matrix is largely elastic, with plasticity confined to a region close to the tip of the crack which has blunted in the matrix. In a situation wherein the matrix yields, but the constraint is still high enough (strong interface and no particle cracking), the stress distribution within the matrix is sensitive to events at the blunt tip and tends to involve relatively high levels of hydrostatic stress, and the load supported by the matrix becomes correspondingly high. If the constraints from the stiffer surrounding reinforcing particle can be relieved sufficiently by crack - tip deformation and/or interfacial debonding, the matrix is allowed to neck at a lower stress level within the particle. Moreover, lower nominal stress levels arise because of the decreased load-bearing area. This regime, however, dominates the later stages of deformation when the matrix fails in a highly ductile manner [48]. A deformation regime that is dominated by the nucleation, growth and coalescence of a single large void or a small number of large voids in the matrix can also be visualised [49]. This deformation mechanism has the effect of lowering the constraint on the ligament and leads to fracture surfaces reminiscent of ductile fracture of the base Al-alloy. This mechanism involves smaller failure separation distances than are seen in a fully ductile failure, although extensive plasticity is involved in necking down of the matrix between the voids.

The toughness enhancement due to bridging, however, is expected to be dominated by the contribution from the necking regime, since the high stresses in the constrained plasticity regime persist only briefly. The toughening enhancement is also dependent on the yield stress and strain hardening of the matrix, unless an associated lack of ductility leads to failure at significantly decreased separation distances. The matrix deformation characteristics to a large extent control the shape of the *R*-curve in the composites. A schematic representation of the observed deformation mode and its influence on $\sigma(u)$ of the matrix and on the R-curve is shown in figure14. The role of microstructural characteristics on the R-curve *may therefore be explained as follows :*

Influence of particle size

The plateau toughness from R-curves values agreed well with the measured fracture toughness values of 11.4 MPa√m and 9.5 MPa√m in composite A (<1μm, V_f ~0.56) and B_1 (3μm, V_f ~0.58) respectively , but were not observed to correlate with the measured values in coarse particle composites. The high plateau toughness of composites observed in *R*-curve *tests* is possibly due to a larger incidence of bridges forming behind the crack front. The highest plateau toughness is reached in a composite with mean particle size of 3μm (composite B_1) and 23μm (composite C_3) although at differing crack extensions. In coarse particulate composites (≥ 23μm), additional effects of microcracking, large stable crack growth and resulting effects of finite specimen geometry lead to plateau toughness at larger *a/W*. Comparing the toughening increment with the crack tip toughness of ~ 4 MPa√m, gives an indication of the significance of fracture energy contribution from the matrix. The bridging matrix deformation characterised by limited interfacial debonding and initiation of a single void (P ~ 2-4) is expected to be energy intensive as compared to deformation by extensive void nucleation, growth and coalescence (P ~ 1) accounting for the sharp rise to plateau peak toughness.

Influence of particle volume fraction

With increase in particle volume fraction, a marked reduction in the measured fracture toughness and plateau toughness (*R*-curve analysis) were observed. The reduction in toughness is directly attributed to the reduced volume fraction of the bridging matrix ligaments; thus, higher plateau toughness at larger *a/W* was observed in composites with a moderate alumina volume fraction of 47-61%. Composites with higher volume fraction of ceramic (~75%), showed reduced fracture toughness and peak toughness values. The large deviation of plateau toughness from measured fracture toughness values *that is* observed in composites with moderate reinforcement volume fractions (47-61%) can be related to the deformation behaviour of the bridging matrix ligaments. In composites with volume fraction of ~ 75%, the matrix showed failure by deforming as well formed ridges (Fig. 11 f), however, failure in composites with reduced volume fraction (36-60%) showed extensive striations typical of slip bands (Fig. 11 c). The slip bands are possibly activated by reduction in constraint, and influence the critical strain to failure of the bridging matrix ligaments. The fracture energy consumed in the first case is much lower than when the second condition prevails, and the matrix ligaments are observed to fail at higher plastic stretch in the lower volume fraction when compared to composites with very high volume fraction of particles.

Toughness modelling

As seen from the table 2 and the plot of the *measured and calculated* steady state toughnesses (Fig. 15), the observed trends reflect the variation in the measured fracture toughness of the composites reasonably well. However, in composites D and E, characterised by large reinforcement particles (75-180μm), large matrix spacing (37-95μm) and failure by extensive void nucleation in the matrix, the calculated toughness due to the bridging contribution is observed to be overestimated by almost a factor of 2. The overestimation is likely

to be due to two factors. Firstly, the assumption of a uniform matrix size for calculating the matrix contribution to the toughness (equation 4) may not reflect the inherent distribution *whose width is observed to increase with* particle size. Further refining of the model by including a factor defining the distribution is probably justified [50]. Secondly, significant error can be expected by assuming that deformation is uniform throughout the matrix. The experimentally determined u^* is from the matrix that has deformed near the particle and is still affected by the constraint imposed by the particles. However, matrix deformation to failure at lower stress levels and reduced strains is likely to occur at distances significantly away from the particle due to extensive void nucleation. Incorporating these factors in the model should *enable a prediction of composite toughness that is closer* to the measured values. Although the bridging model as applied here is able to predict the composite toughness at a steady state of bridging it does not reveal information regarding the shape of the *R*-curve or on the crack growth required to reach steady state toughness. Thus the independently measured K_Q is either the steady state toughness of the material or is an intermediate value prior to reaching steady state, depending on the shape of the K_R - curve. A model capable of predicting the variation of measured K_Q with measured steady state toughness, K_{SS} , and the crack growth required for achieving K_{SS} thus assumes much significance.

From the computed crack tip profile, the measured values of K_Q are analysed to be within the range of steady state toughness regime by plotting the critical COD to failure $2u^*$ at a constant Δc of 600 μm (pre-crack length in K_Q analysis). As shown in figure 14 only a few of the calculated COD $2u^*$ corresponding to composites with fine microstructure, high reinforcement volume fraction or processed at high temperatures, lie within or very close to the bounds. Within the experimental error, these values can be assumed to correspond to the steady state toughness values from the K_R - curves. But in composites, wherein the COD $2u^*$ was observed to lie further away from the computed bounds, it is imperative that the measured K_Q bears no relation to the steady state toughness of the material which is reached at large

increments of crack growth. This is in concurrence with the observed shape of the K_R - curves in the composites. Calculation of the bridge length further strengthens the analysis in predicting that in composites with a very fine microstructure the steady state toughness was reached at a bridge length of < 0.2 mm. which is small compared to the overall crack length c_e {initial crack c_o (= 2.4 mm.) + bridging zone length, L}. A larger bridge length L of up to 2 mm. that was a significant fraction of the overall crack length c_e, was required to achieve steady state toughness in composites with a relatively coarse microstructure (particle size of 23μm and above and volume fraction ≤ 60%). In composites with a very coarse microstructure (composite D and E), the bridging zone length (L = 5-8 mm.) predicted for reaching steady state toughness is equivalent to the observed crack growth in the specimens (Fig. 16). The bridged crack forms a very large component of the overall crack length and is similar in magnitude to the specimen dimensions (W = 12 mm.). This behaviour is characteristic of large scale bridging (LSB) prevailing in the specimen which necessitates the use of larger specimens for crack growth studies.

Thus based on the extent of crack extension to stabilise or achieve steady-state toughness, the observed K_R - curve behaviour in the composites can be divided into short range and long range toughening behaviour as shown in figure 17.

a) Short range toughening The composites show a sharply rising K_R- curve reaching a plateau after short crack extension. The plateau toughness becomes comparable with the K_Q values obtained by independent fracture toughness measurements.

b) Long range toughening The K_R curves start at very low values and increase continuously with crack growth. The measured K_Q values correspond to the K_R values at intermediate crack extension. This behaviour also shows a very short plateau region (quasi-plateau) prior to fracture

CONCLUSIONS

Fracture toughness and fracture mechanisms have been studied in Al_2O_3 / (Al -AlN) composite processed by pressureless infiltration of molten Al-alloys into alumina preforms. The *flexibility of the process technique enables the fabrication of composites with a microstructure ranging from particulate dispersed metal matrix composites to interpenetrating phase composites over a microstructural scale that rises from less than a micron to hundreds of microns*. The microstructural scale exerts a strong influence on the crack resistance of the composites, which increases with crack extension. The crack growth resistance curves begin at the intrinsic toughness of the matrix ~3-4 MPa√m and the mechanism for rise in crack resistance has been identified as crack bridging by intact ductile ligaments in the crack wake. The rate of increase in crack resistance upon crack extension and the final resistance reached prior to failure is controlled by the microstructure viz. size, volume fraction and deformation characteristics of the metal ligament. The ligament deforms to failure with the nucleation of a single void in the matrix (high constraint); nucleation of voids at the centre and/or near the interface (moderate constraint) and by extensive nucleation of voids in the matrix (low constraint).

The rate of increase in crack resistance with crack extension, the bridge zone formed and the final steady state toughness of the composites can be predicted from known micro-mechanical models incorporated with experimentally measured constraints on the deforming ductile ligament and the final elongation prior to failure. From the observed and predicted crack resistance, the composites can be classified as short range toughened (fine microstructure and high ceramic volume fraction) and long range toughened (coarse microstructure and low ceramic volume fraction). The flexibility in the process technique offers a new route for the designing of composites with controlled macro/microstructures to have a favourable combination of short crack and long crack toughness

ACKNOWLEDGEMENTS

The authors would like to acknowledge A.H Chokshi, M.K. Surappa and B. Dutta, all of Department of Metallurgy, Indian Institute of Science for their help in the use of Instron and dynamic measurements of hardness, respectively, and C.R.L Murthy and M.R. Bhat from the Department of Aerospace Engineering for their help in measurements of elastic modulus. Financial support for the present work was provided by the Board of Research Nuclear Sciences, Government of India

REFERENCES

1. M.S. Newkirk, A.W. Urquhart and H.R. Zwicker, *J. Mater. Res*. **1,** 81, (1986)
2. M.K. Aghajanian, N.H. Macmillan, C.R. Kennedy, S. J. Luszcz and R. Roy*, J. Mater. Sci*., **24** , 658 (1989)
3. S. Antolin, A.S. Nagelberg and D.K. Creber, *J. Am. Ceram. Soc*. **75**, 447 (1992)
4. M. Hanabe, V. Jayaram and T.A. Bhaskaran, *Acta mater*. **44**, 819 (1996)
5. S. P. Dhandapani, V. Jayaram and M.K. Surappa, *Acta Mater*. **42**, 649 (1994)
6. W.G. Fahrenholtz, K.G. Ewsuk, R.E. Loehman and A.P. Tomasia, "*In-situ Reactions for synthesis of Composites, Ceramics and Intermetallics*" The Minerals, Metals and Materials Society, 99 (1995)
7. R.E. Lochmann, K. Ewsuk and A.J. Tomasia, *J. Am. Ceram. Soc*. **79**, 27 (1996)
8. M.C. Breslin, J. Rignalda, L. Xu, M. Fuller, J. Seeger, G.S. Daehn and H.L. Fraser, *Mater. Sci. Eng*. **195A** , 113 (1995)
9. P.K Balasubramanian, P.S. Rao, B.C. Pai , *Composites Sci. and Tech*. **39**, 245 (1990)
10. A. Mortensen, M.N. Gungor, J.A. Cornie and M.C. Flemings, *J. Metals*, **38**, 30 (1986)
11. G. Bao and F. Zok, Acta metall. mater. 41, 3515 (1993)
12. F. Erdogan and P.F. Joseph, J. Am. Ceram. Soc., 72, 262 (1989)
13. L.S. Sigl, P.A. Mataga, B.J. Dalgleish, R.M. McMeeking and A.G. Evans, *Acta. metall*. **36**, 945 (1988)
14. Tattersall and G. Tappin, J. Mater. Sci., 1 296 (1966)
15. G.K. Bansal, W.H. Duckworth and D.E. Niesz, J. Am. Ceram. Soc., 59, 472 (1976)
16. R.F. Pabst, `Fracture Mechanics of Ceramics' eds. R.C. Bradt, D.P.H. Hasselman and F.F. Lanfe, Plenum Press, New york. Vol 2. 555 (1974)
17. B. Mussler, M.V. Swain and N. Claussen, J. Am. Ceram. Soc., 65, 566 (1982)
18. J.L. Shannon, Jr., and D.G. Munz, ASTM STP 855, eds. J.H. Underwood, S.W. Freiman and F.I. Barrata, , American Society for Testing and Materials, Philadelphia, PA 270 (1984)

19. R.F. Cook, B.R. Lawn and C.J. Fairbanks, J. Am. Ceram. Soc., 68, 604 (1985)

20. F.W. Zok and C.L. Hom, Acta metall. mater. 38, 1895 (1990)

21. J. Rödel, J.F. Kelly and B.R. Lawn, J. Am. Ceram. Soc., 73, 3313 (1990)

22. M. Hoffman, B. Fiedler, T. Emmel, H. Prielipp, N. Claussen, D. Gross and J. Rödel, Acta mater. 45, 3609, 1997

23. Thompson and R. Raj. Acta metall. mater., 42, 2477 (1994)

24. S.M. Pickard, E. Manor. H. Ni, A.G. Evans and R. Mehrabian, Acta Metall. Mater., 40, 177 (1992)

25. S J. Rödel, M. Sindel, M. Dransmann, R.W. Steinbrech and N. Claussen, J. Euro. Ceram. Soc. 14, 153, (1994)

26. B.D. Flinn, M. Rühle and A.G. Evans, Acta Metall. 37 3001 (1989)

27. H. Prielipp, M. Knechtel, N. Claussen, S.K. Streiffer, H. Müllejans, M. Rühle and J. Rödel, *Mat. Sci. and Eng*. **197A,** 19 (1995)

28. D.T. Ellerby, B.D. Flinn, W.D. Scott and R.K. Bordia, Proceedings of ICCM-10, Whistler, B.C., Canada, (1995)

29. D.K. Creber, S.D. Poste, M.K. Aghajanian and T.D. Claar, *Proc. Ceram. Engg. Sci*., **9** , 447 (1988)

30. M.K. Aghajanian, J.T. Burke, D.R. White and A.S. Nagelberg, *SAMPE Quarterly*, **20**, 43 (1989)

31. M.K. Aghajanian, M.A. Rocazella, J.T. Burke, S.D. Keck, *J. Mater. Sci*. , **26,** 447 (1991)

32. M.K. Aghajanian , R.A. Langensiepen, M.A. Rocazella, J.T. Leighton and C.A. Andersson, *J. Mater. Sci*., **28 ,** 6683 (1993)

33. E. Breval, M.K. Aghajanian, J.P. Biel and S. Antolin, *J. Am. Ceram. Soc*., **76** , 1865 (1993)

34. N. Nagendra, Ph.D Thesis, Indian Institute of Science (1997)

35. T. Nose and T. Fujii, *J. Am. Ceram. Soc*. **71**, 328 (1988)

36. A. Saxena and S. J. Hudak Jr., *Int. Jl. Fract*. **14**, 5 (1978)

37. K.L. Johnson, *J. Mech. Phys. Solids* **18**, 115 (1970)

38. J.W. Leggoe, X.Z. Hu, M.V. Swain and M.B. Bush, *Scripta. metall. mater*. **31**, 577 (1994)

39. G. Bao and C.Y. Hui, Int. J. Solids. Struct., 26, 631 (1990)

40. B.D. Flinn, C.S. Lo, F.W. Zok and A.G. Evans, *J. Am. Ceram. Soc*. **76** , 369 (1993)

41. M.F. Ashby, F.J. Blunt and M. Bannister, *Acta. metall*. **37**, 1047 (1989)

42. H.E. Déve, G.R. Odvette, R. Mehrabian, R.J. Hecht and A.G. Evans, *Acta. metall*. **38**, 491 (1990)

43. poisson

44. G.R. Irwin, *"Fracture"* **94**, Handbuch der Physics, Springer-Verlag, Berlin, 551 (1958)

45. V.D. Kristic, *Philos. Mag. A* **48**, 695 (1983)

46. D.J. Lloyd, H.P. Lagace and A.D. McLeod, Controlled Interphases in composite materials, ed. H. Ishida, Elsevier Science Publishing Co., Inc, 359 (1990)

47. J.K. Shiang and R.O. Ritchie, Metall. Trans A, 20A 897 (1989)

48. P.A. Mataga, Acta metall. 37, 3349 (1989)

49. L.S. Sigl and H.K. Exner, Metall. Transa A, 18 A, 1299 (1987)

50. X. Sun and J.A. Yeomans, *J. Am. Ceram. Soc*. **79** , 562 (1996)

FIGURES

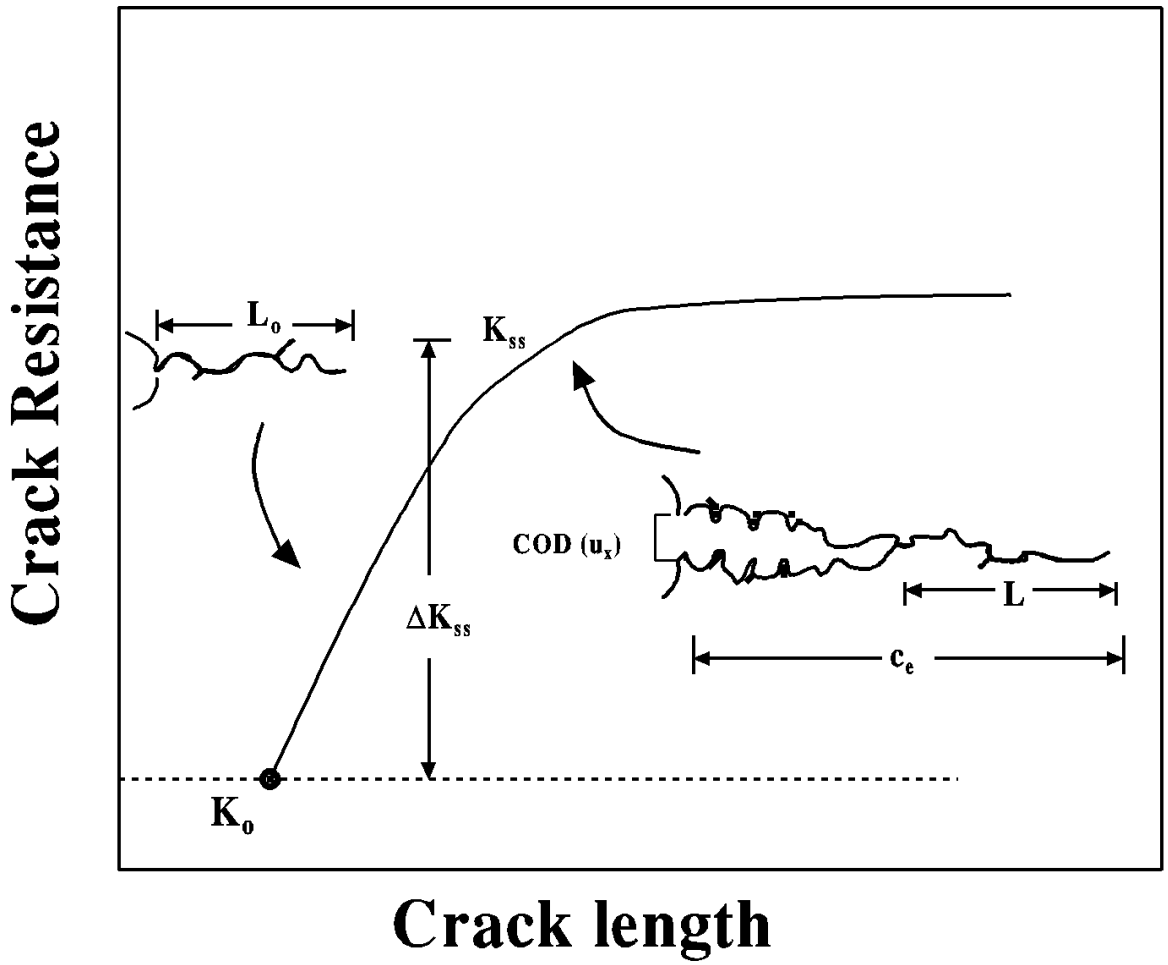

Fig. 1 **Schematic representation of a bridged crack and its relation to Crack opening displacement (COD)**

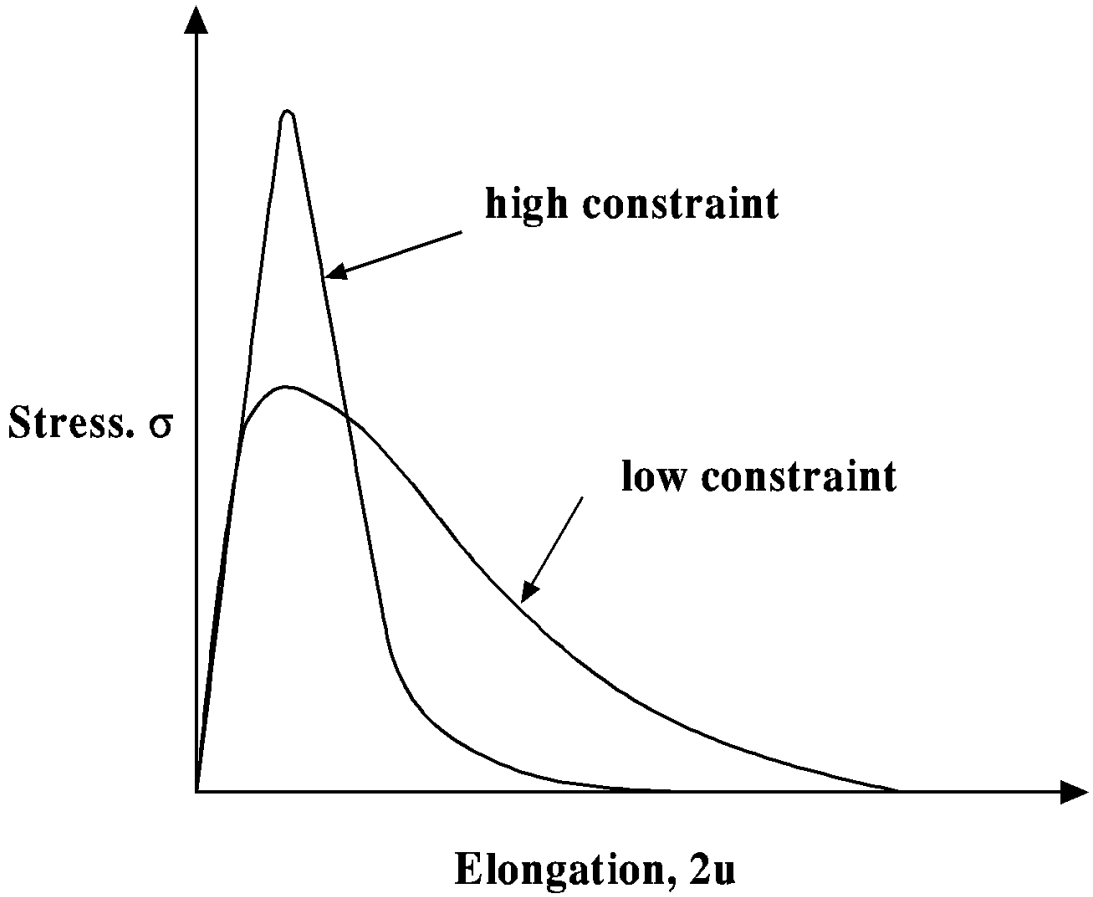

Fig. 2 **Deformation characteristics of ductile phase under constrained condition**

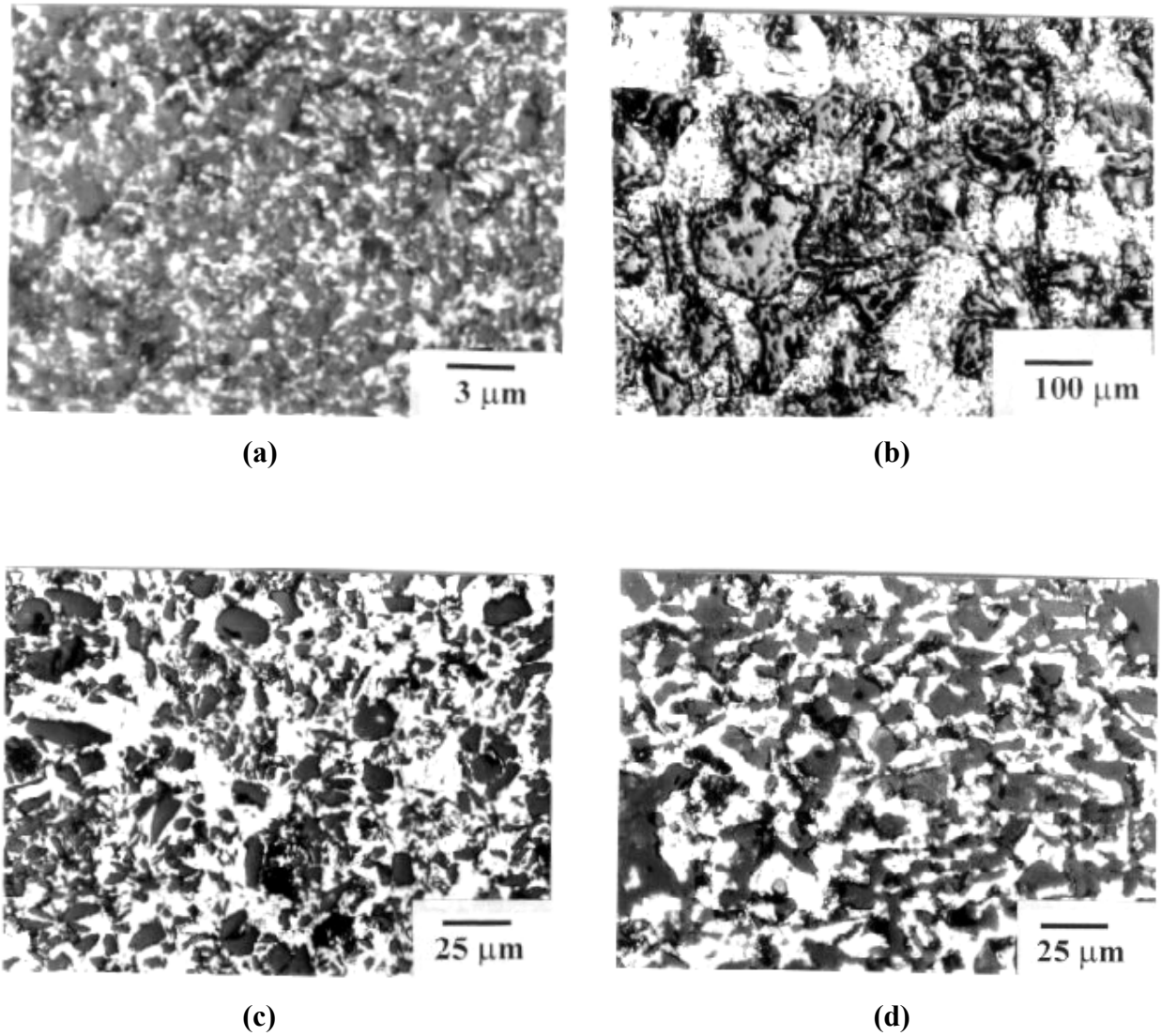

Fig. 3 **Microstructure of composites studied with variation in : i) particle size (a-b) and ii) volume fraction (c-d)**

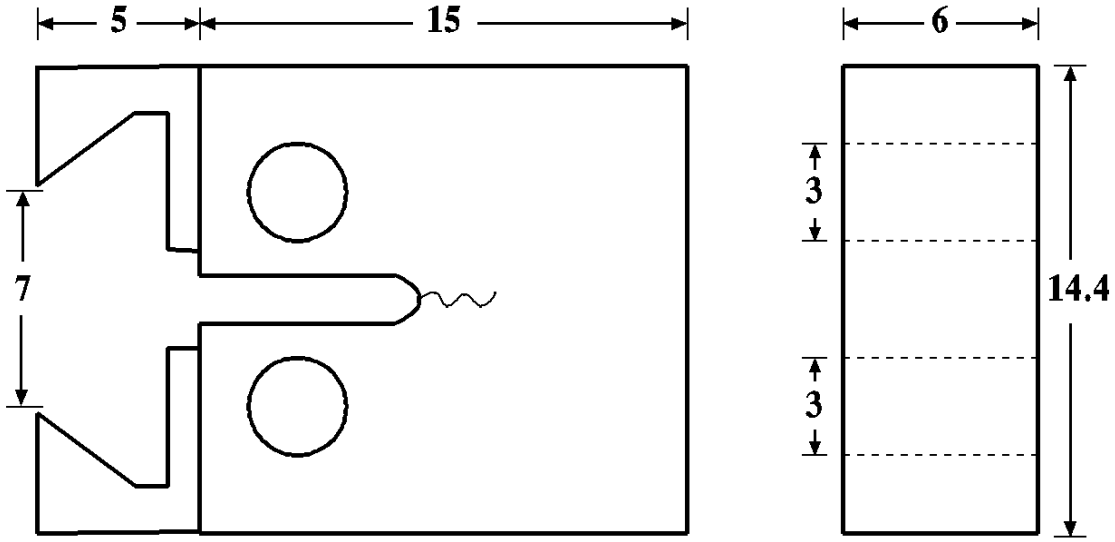

Fig. 4 **Compact tension sample for fracture toughness and *R*-curve studies. (Dimensions in mm.)**

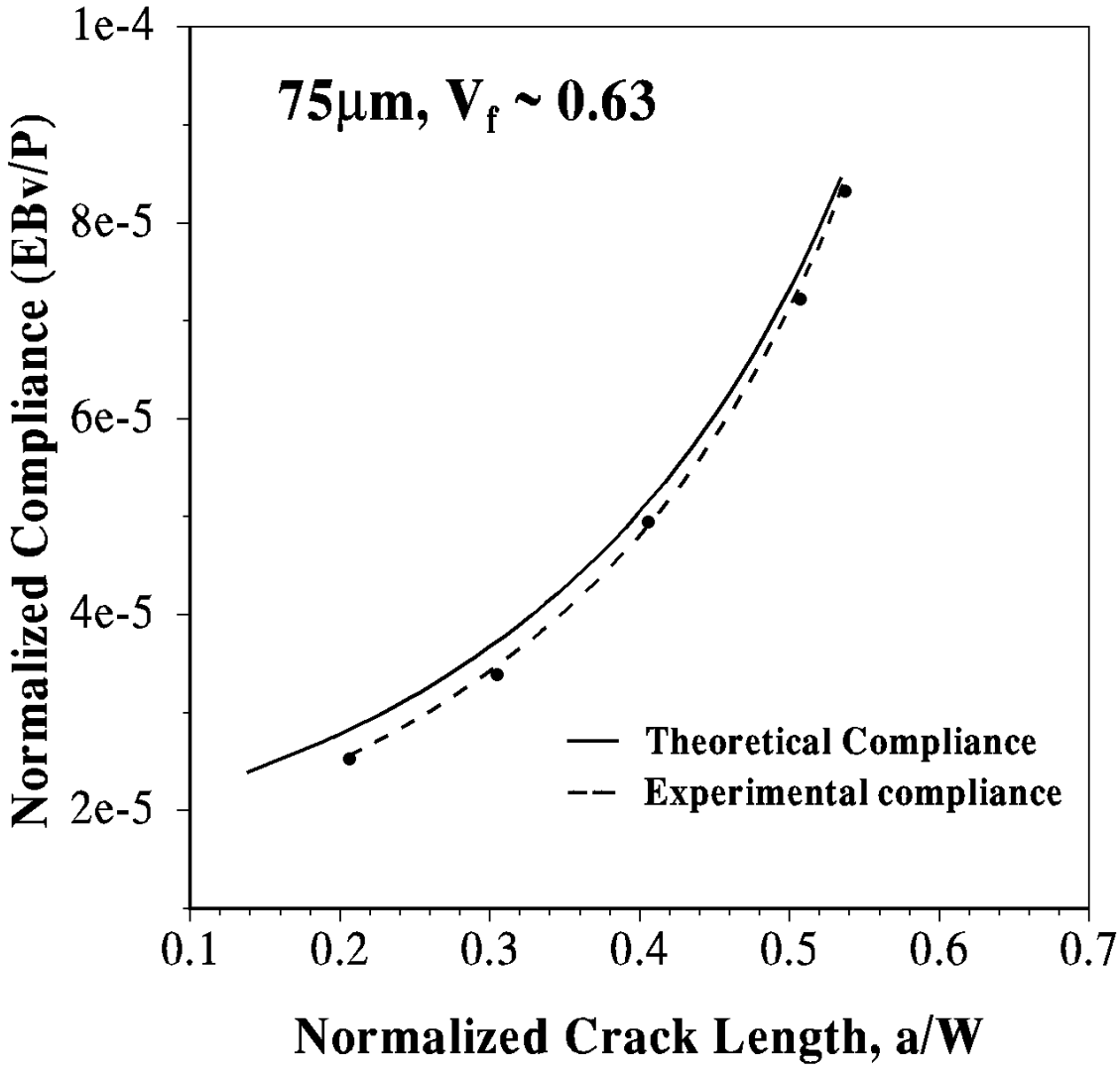

Fig. 5 Typical compliance calibration curve for predicting crack length in composites.

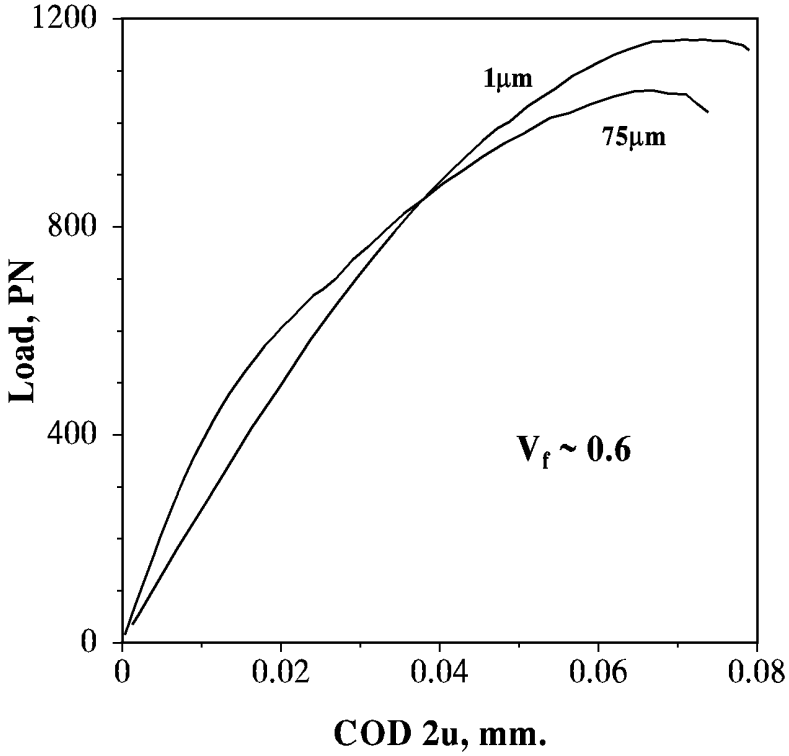

Fig. 6 Typical load vs. COD curves for composites with 1 and 75 μm particulate

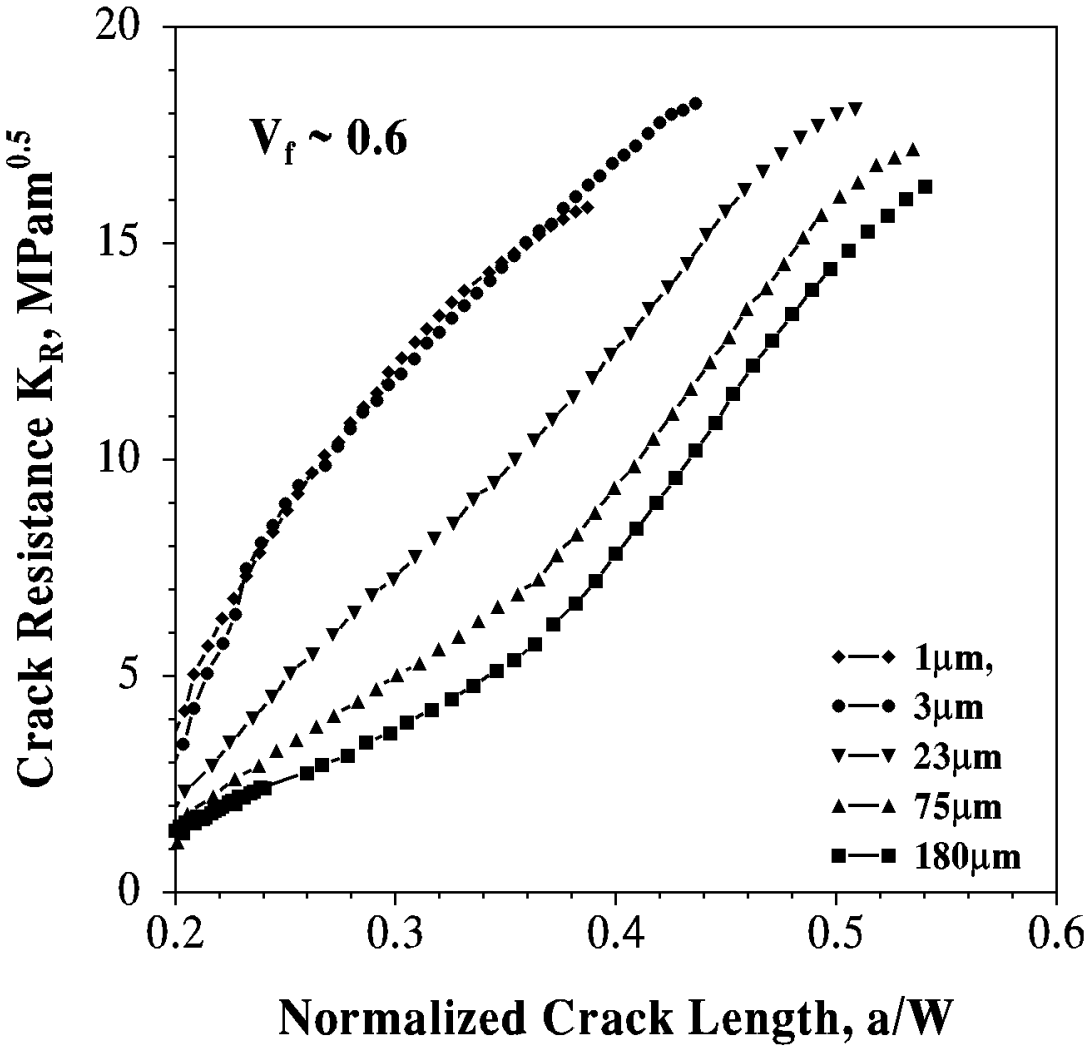
20
15
10
5
0
0.2
0.3
0.4
0.5
0.6
V_f ~ 0.6
Crack Resistance K_R, MPam$^{0.5}$
Normalized Crack Length, a/W
1μm,
3μm
23μm
75μm
180μm

Fig. 7 a)

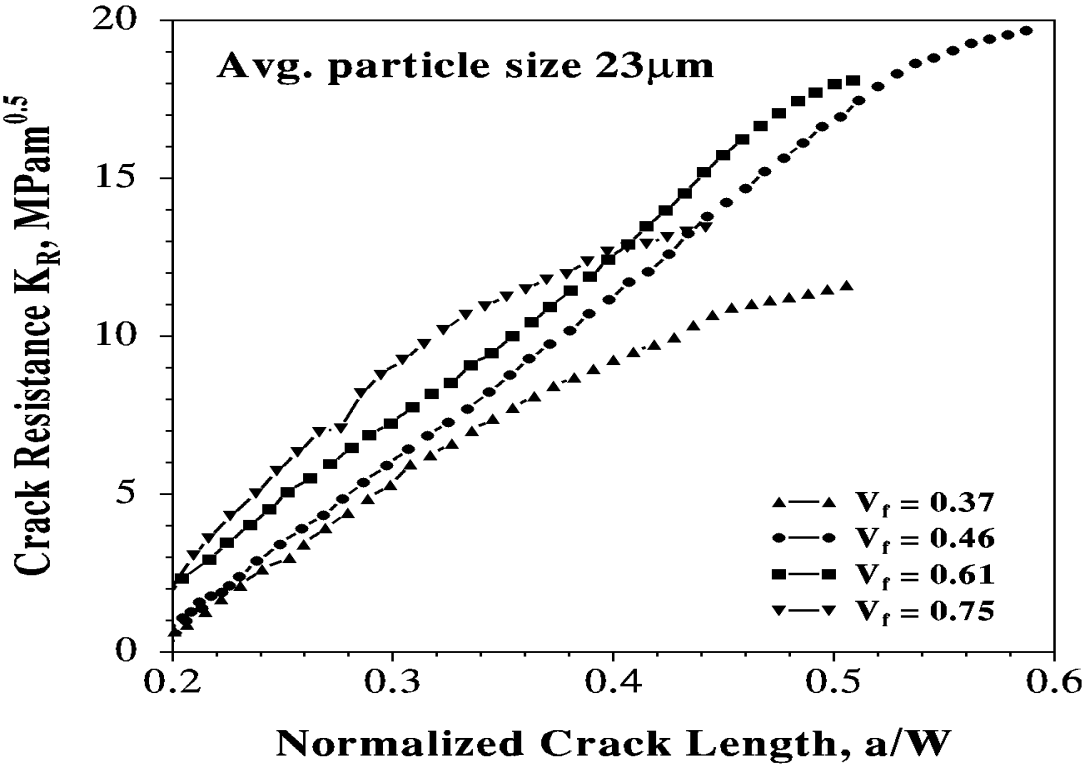

Fig. 7 b)

Fig. 7 **Rise in crack resistance with crack extension in composites with variation in a) particle size and b) particle volume fraction,**

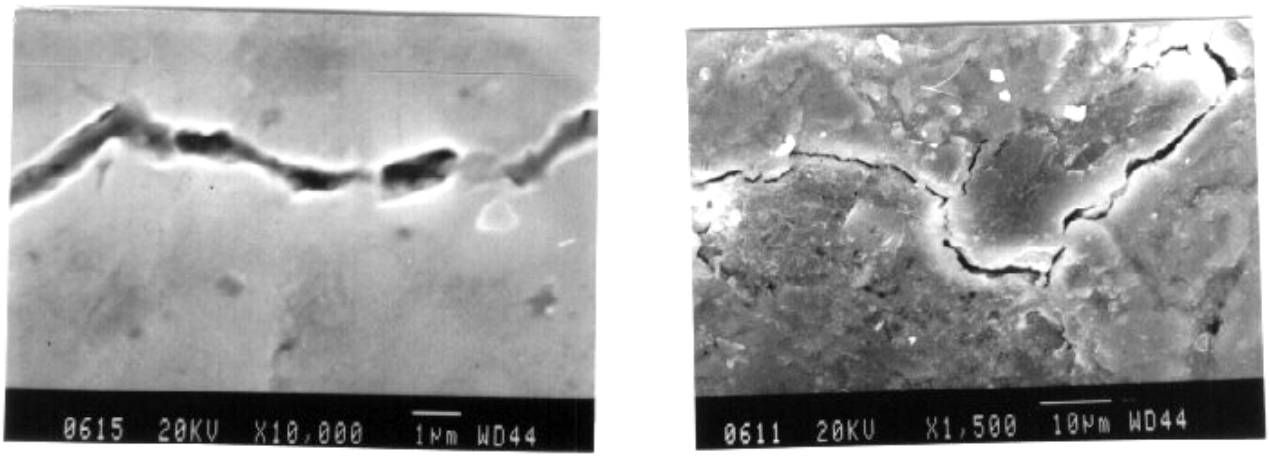

a) **b)**

Fig. 8 **Bridged cracks in a) fine microstructured composites and b) coarse microstructured composites.**

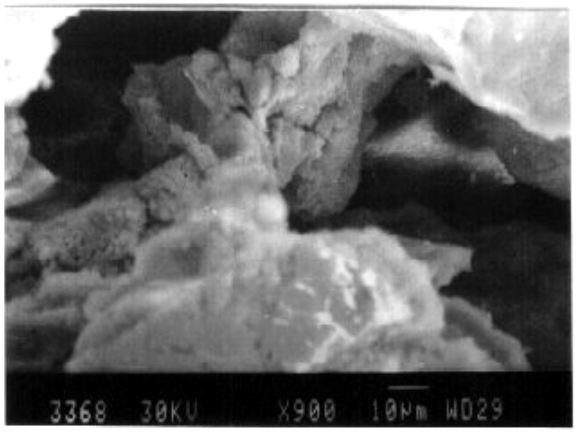

Fig. 9 **Deformation of the intact matrix bridging the two crack faces behind the crack tip**

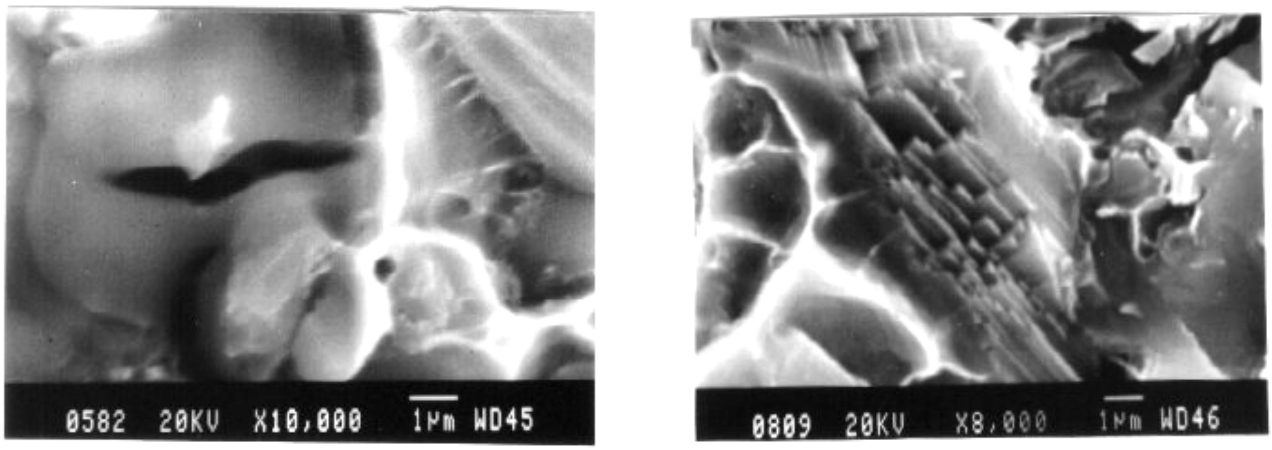

a) **b)**

Fig. 10 **Particle fracture observed in the composites : a) interfacial failure with particle cracking and b) cleavage fracture in coarse particle**

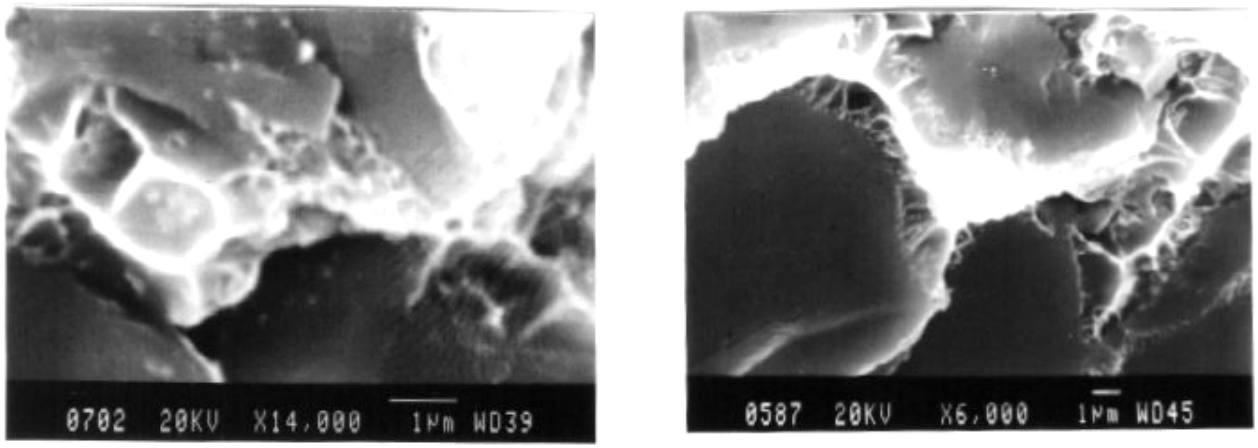

a) **b)**

Fig. 11 **Changes in deformation and failure modes in the matrices with changes in plastic constraint factor : a-b) by void nucleation at the centre of the matrix (high constraints, P ~ 2-4); c-f) Activation of slip bands and voids nucleation in the matrix (moderate constraint, P ~ 1.4-2); g) preferential void nucleation at near the interface (low moderate constraint, P ~ 1.3); extensive void nucleation in the matrix (low constraint, P ~ 1)**

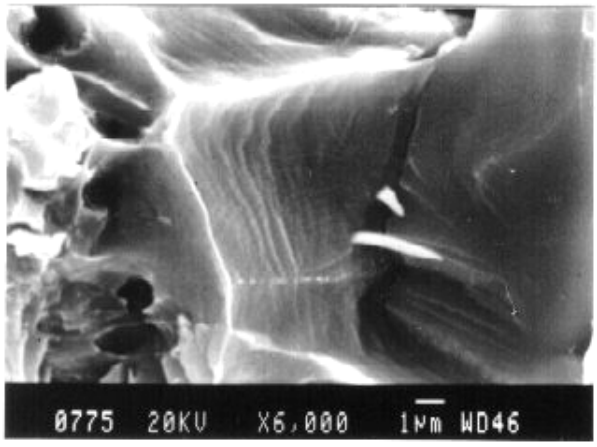

c)

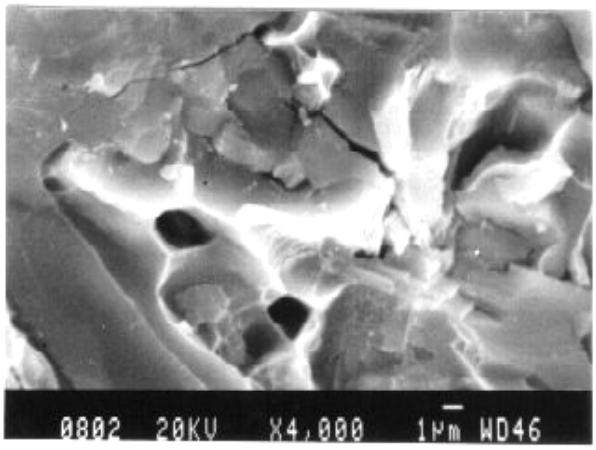

d)

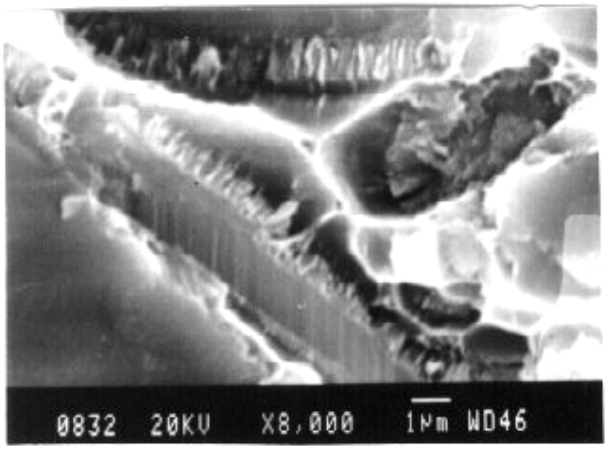

e)

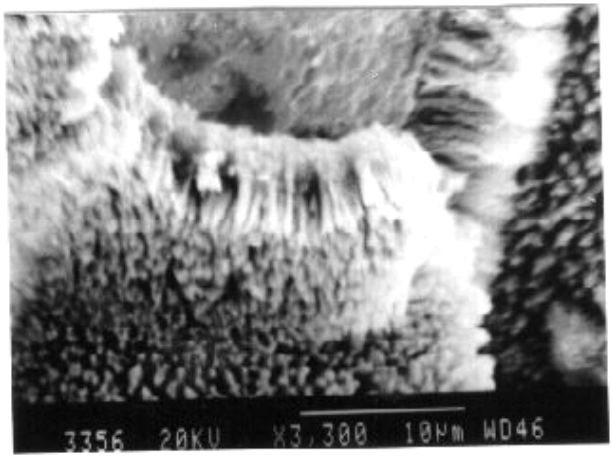

f)

Fig. 11 **Changes in deformation and failure modes in the matrices with changes in plastic constraint factor : a-b) by void nucleation at the centre of the matrix (high constraints, P ~ 2-4); c-d) Activation of slip bands and voids nucleation in the matrix (moderate constraint, P ~ 1.4-2); e) preferential void nucleation at near the interface (low moderate constraint, P ~ 1.3); f) extensive void nucleation in the matrix (low constraint, P ~ 1)**

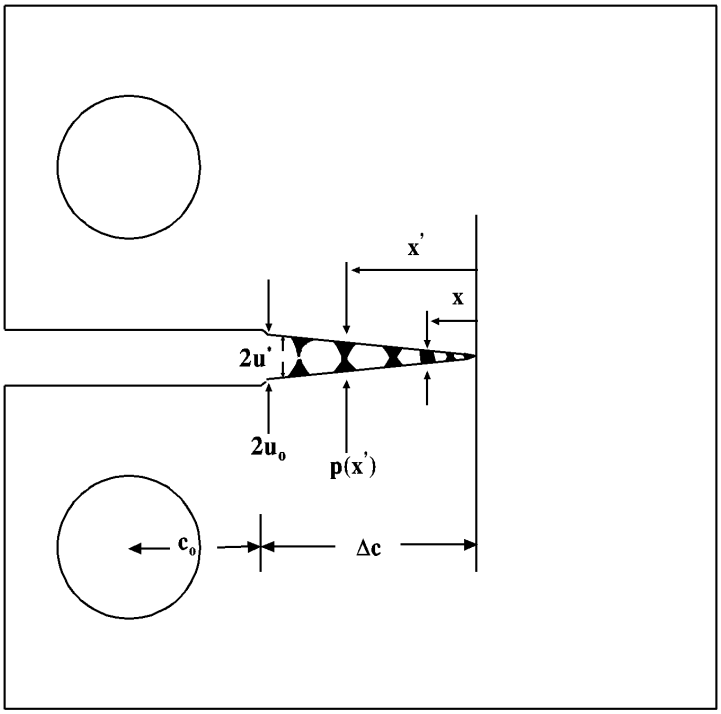

Fig. 12 **Schematic representation of bridging parameters and experimental measurement of critical crack opening displacement (2u*) in CT test specimen.**

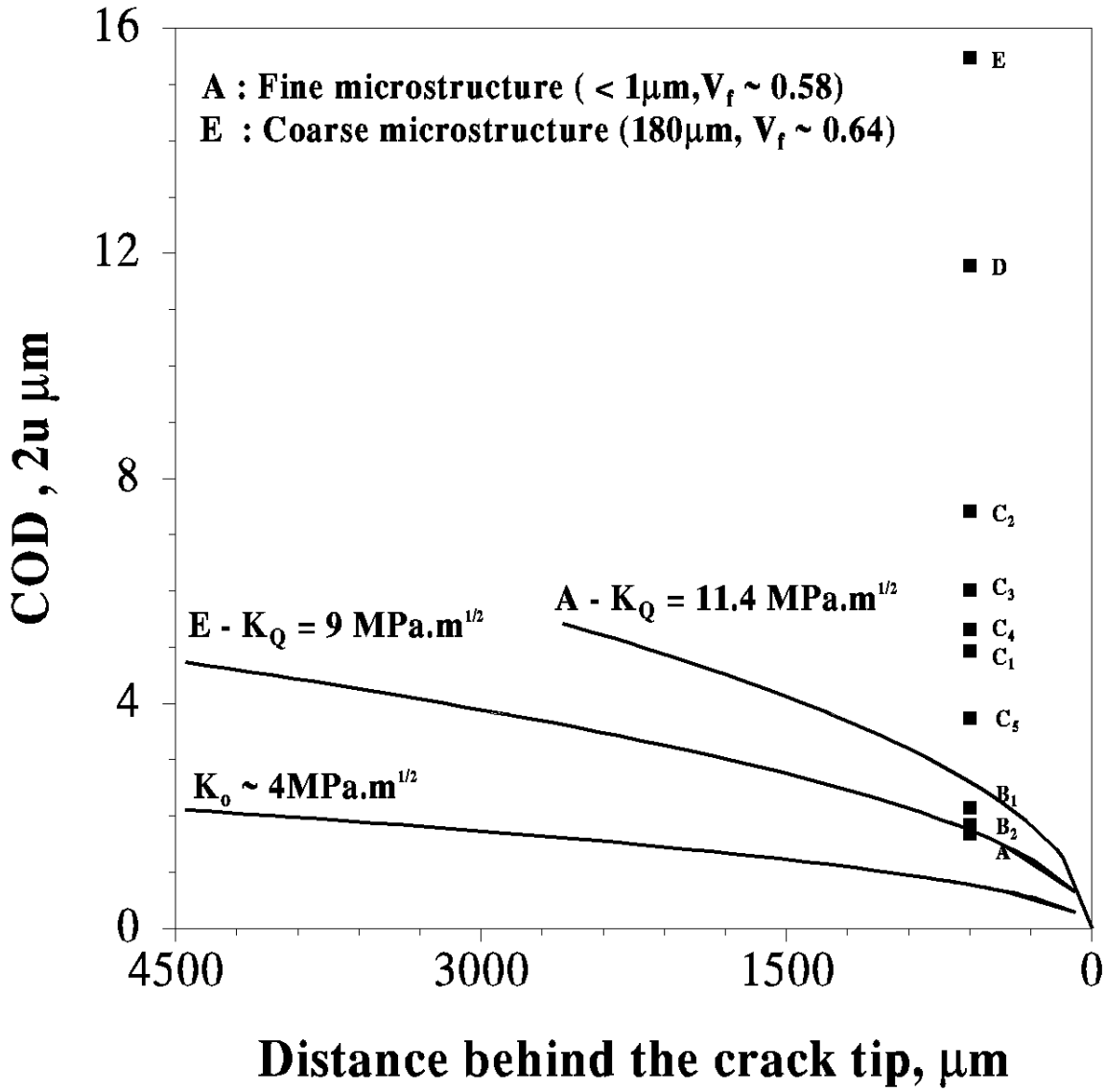

Fig. 13 **Theoretically computed COD as a function of distance behind the crack tip. The critical extension to failure, 2u*, of the matrix ligament is plotted at a distance of 600μm corresponding to precrack length for fracture toughness studies.**

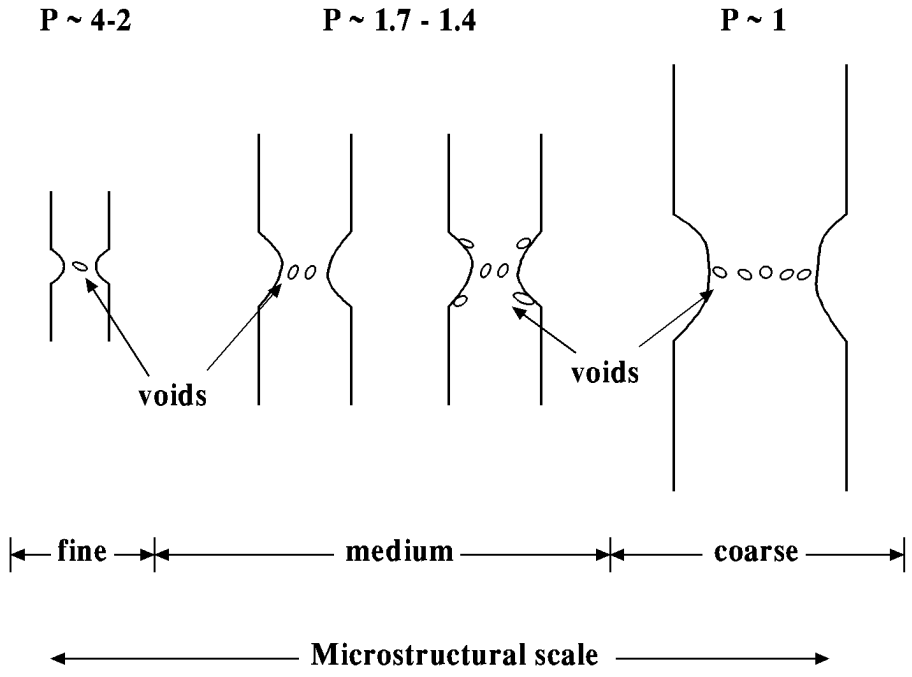

Fig 14 a)

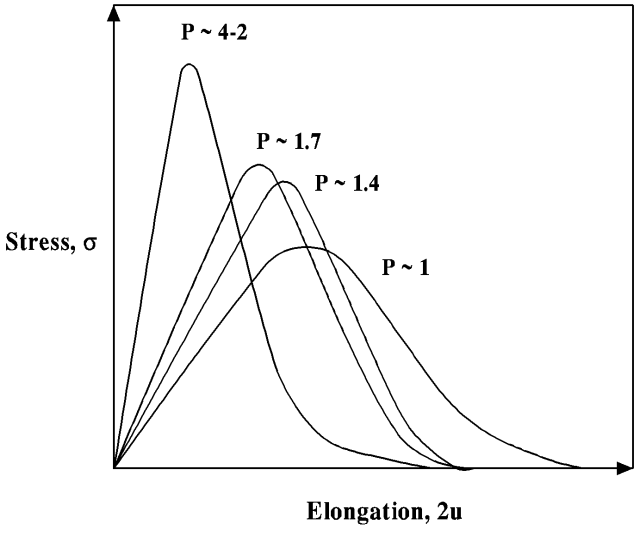

Fig 14 b)

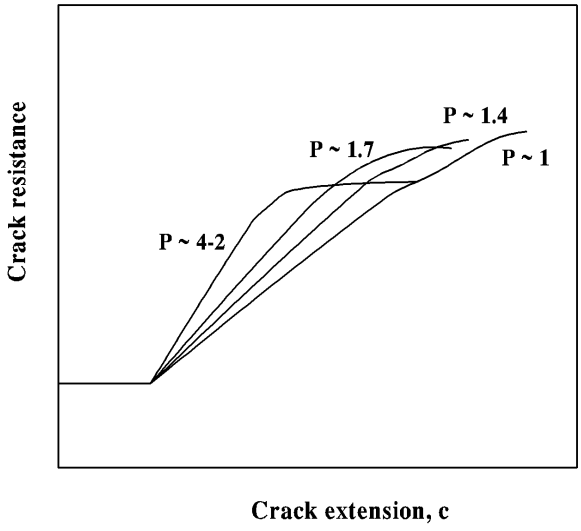

Fig 14 c)

Fig. 14 **Deformation modes as a function of the microstructural characteristics and their influence on the σ(u) curves of the matrix (b) and on the R-curves of the composites(c).**

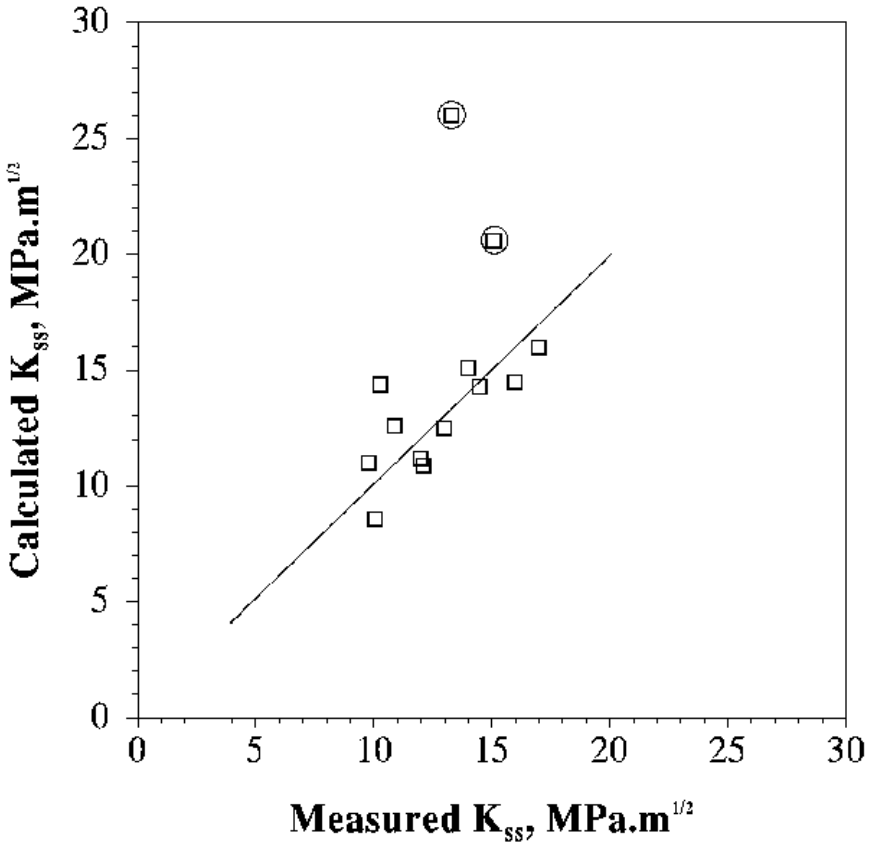

Fig. 15 **Calculated and measured steady state toughness K_{SS} in the composites studied**

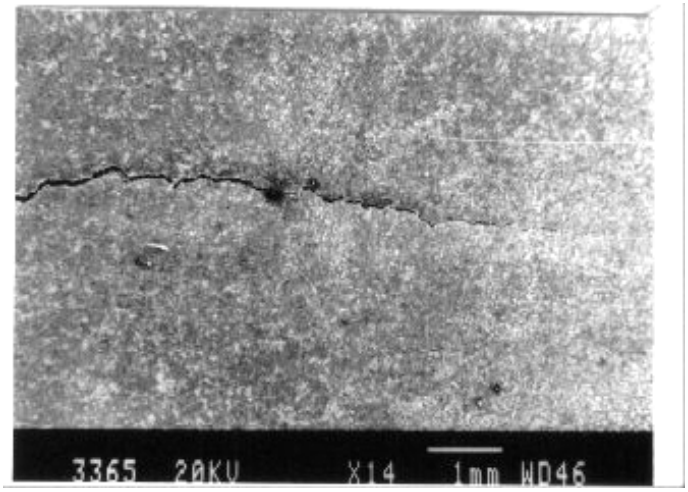

Fig. 16 **A bridged crack extending over several mm. observed in coarse particulate composites**

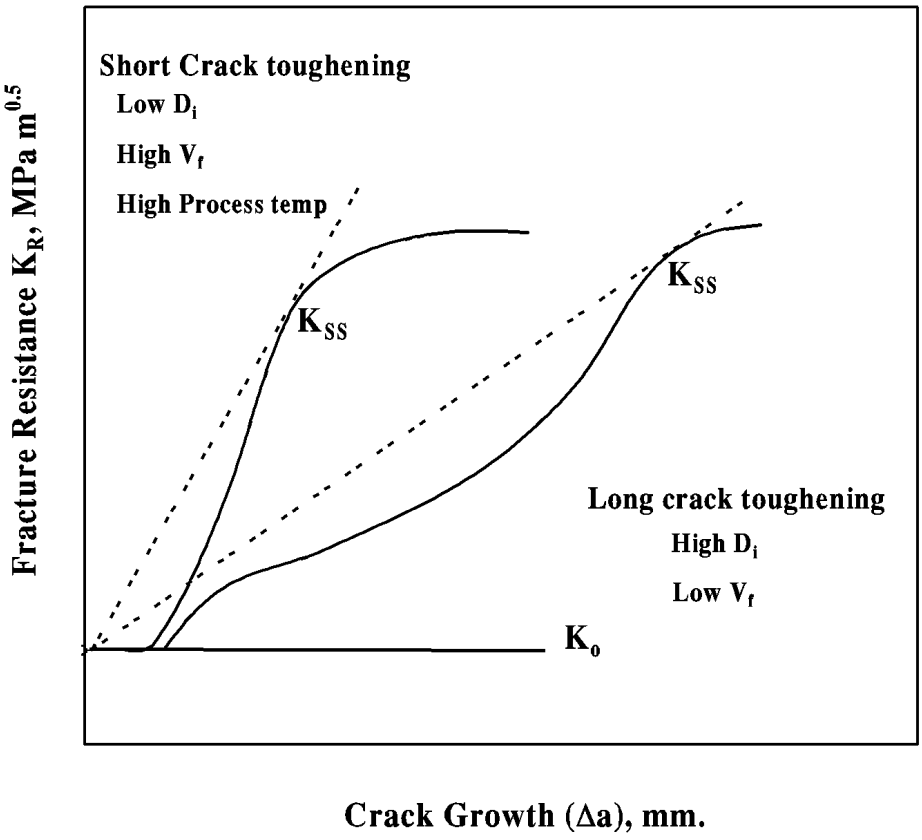

Fig. 17 **Schematic of R-curve behaviour observed in the composites with respect to its microstructural characteristics.**

TABLES

Table 1 **Relative plastic constraint experienced by the matrix as a function of microstructural parameters**

		d_i, μm	V_f	λ_i, μm	E GPa	K_Q MPa√m	h_i, μm	c_i, μm	Plastic Constraint (P)
Base metal					69	18	0.25	1.98	
							1.73	13.72	
Particle size									
Composite	**A**	1	0.56	0.8	158	11.4	0.07	0.61	3.24
	B_1	3.79	0.58	1.1	166	9.5	0.10	0.82	2.41
	C_3	23	0.61	8.9	195	10.7	1.24	9.83	1.40
	D	75	0.63	37.5	193	9.2	1.27	10.09	1.36
	E	180	0.64	95	187	9	1.32	10.49	1.31
Aspect ratio									
Composite	**B_1**	3.79	0.58	1.1	166	9.5	0.10	0.82	2.41
	B_2	3/0.3	0.58	1.27	174	9.3	0.16	1.32	1.51
Volume Fraction									
Composite	**C_1**	23	37	13	134	11.5	1.25	9.93	1.38
	C_2	23	46	11.5	147	15.8	1.26	9.97	1.38
	C_3	23	61	8.9	195	10.7	1.24	9.83	1.40
(calcined)	**C_4**	23	75	8.5	241	9.8	1.20	9.52	1.44
(fused)	**C_5**	23	76	7.2	233	10.3	1.04	8.25	1.66

Table 2 Comparison of calculated and experimentally measured steady state toughness

Composites		Matrix strength, σ_y MPa ($P\sigma_o$)	u*, μm	Measured K_{SS}, MPa√m	Calculated K_{SS}, MPa√m	Bridging Zone, L, mm.	L/c
Particle size							
Composite	**A**	894	0.84	12	11.2	0.10	0.04
	B_1	665	1.07	9.8	11	0.16	0.06
	C_3	387	3.01	16	14.5	1.33	0.36
	D	375	5.89	15.1	20.6	5.10	0.68
	E	362	7.74	13.3	26	8.82	0.78
Aspect ratio							
composite	**B_1**	665	1.07	9.8	11	0.16	0.06
	B_2	417	0.92	10.1	8.6	0.12	0.05
Volume fraction							
composite	**C_1**	381	2.47	10.3	14.4	0.89	0.27
	C_2	381	3.71	17	16	2.02	0.45
	C_3	387	3.01	16	14.5	1.33	0.36
calcined	**C_4**	397	2.66	10.9	12.6	1.04	0.30
fused	**C_5**	458	1.87	12.1	10.9	0.51	0.18

LIST OF FIGURES

LIST OF TABLES